PNAS RESEARCH ARTICLE | PHYSICS

Shaking and pushing skyrmions: Formation of a nonequilibrium phase with zero critical current

Felix Rucker[a,1], Alla Bezvershenko[b,1], Denis Mettus[a], Andreas Bauer[a,c], Markus Garst[d,e], Achim Rosch[b], and Christian Pfleiderer[a,c,f,g,2]

Affiliations are included on p. 6.

Edited by Stuart Parkin, Max Planck Institute of Microstructure Physics, Halle (Saale), Germany; received March 30, 2025; accepted November 25, 2025

In three-dimensional chiral magnets, skyrmions are line-like objects oriented parallel to the applied magnetic field. The efficient coupling of magnetic skyrmion lattices to spin currents and magnetic fields permits their dynamical manipulation. Here, we explore the dynamics of skyrmion lattices when slowly oscillating the field direction by up to a few degrees on millisecond timescales while simultaneously pushing the skyrmion lattice by electric currents. The field oscillations induce a shaking of the orientation of the skyrmion lines, leading to a phase where the critical depinning current for translational motion vanishes. We measure the transverse susceptibility of MnSi to track various depinning phase transitions induced by currents, oscillating fields, or combinations thereof. An effective slip–stick model for the bending and motion of the skyrmion lines in the presence of disorder explains main features of the experiment and predicts the existence of several dynamical skyrmion lattice phases under shaking and pushing representing phases of matter far from thermal equilibrium.

condensed matter | nonequilibrium | magnetic skyrmions | magnetic susceptibility | MnSi

Significance

Defects and disorder often limit the exploration of the dynamical properties of materials. In magnets, they lead to the pinning of domain walls and other topological defects. We present an experimental and theoretical study of a lattice of magnetic whirls, or skyrmions, driven by electric currents and a slow, periodic shaking of their orientation via an oscillating magnetic field. This shaking overcomes disorder, enabling motion under arbitrarily small forces. As a result, a rich dynamical phase diagram emerges, where skyrmion movement resembles walking and running. Our findings reveal a strikingly simple phenomenon in magnetic materials, providing a controlled platform to explore nonequilibrium dynamical order.

Collective dynamical patterns are ubiquitous in nature, appearing in electronically ordered phases, chemical systems, biological cells, neural networks, and even social contexts. In magnetic materials a particularly rich variety of static patterns has been reported such as conventional magnetic domains (1), quantum order (2–4), and topological textures such as skyrmions, merons, and hopfions (5, 6). This raises the question for the existence and potential properties of collective dynamical patterns among the vast range of magnetic systems which is amenable for theoretical and experimental exploration.

The criteria to be met by a magnetic model system of collective dynamical patterns comprise well-understood forces underlying their formation, and a well-developed theoretical framework providing meaningful insights into the dynamical response. Topological spin textures meet these requirements in an ideal manner. Along with the initial discovery of skyrmion lattices in cubic chiral magnets (7, 8), several key characteristics were reported entailing a search for dynamical patterns. In these materials skyrmions, i), stabilize parallel to an applied field except for tiny corrections by magnetic anisotropies (9, 10), ii) feature an exceptionally strong coupling to spin currents as inferred initially from ultrasmall critical current densities, $j_c \approx 10^6\,\mathrm{Am}^{-2}$ (11–13), iii), display a tiny coupling to disorder and defects as reflected also in the low values of j_c (14–16), and iv), are remarkably well-described using phenomenological modeling (17, 18).

It was, hence, long known that skyrmion lattices in the presence of a current feature two qualitatively different states. First, a static phase where skyrmions do not move, up to corrections from thermal creep (19, 20), and, second, a dynamic phase in which skyrmions are unpinned and flow with a finite average velocity. However, considering that skyrmions in cubic chiral magnets were found to align parallel to the applied magnetic field to minimize their free energy, it was appreciated that changes of the direction of the magnetic field offer an alternative way to manipulate skyrmion strings. Indeed, so-called time-involved small-angle neutron scattering (TISANE) demonstrated the unpinning of the skyrmion lattice under slow, periodic changes of field orientation above a tiny critical angle of ∼0.4° (21, 22). This raises the question addressed in our study, if dynamical skyrmion lattice phases can be accessed and created when combining the effects of pushing by spin currents with shaking the orientation of the skyrmion lattices dynamically.

Key for the exceptionally strong coupling of skyrmions to spin currents are well-understood nonvanishing Berry phases picked up when electrons or magnons traverse a skyrmion (11, 12, 23, 24). Cast in the framework of an emergent electrodynamics,

Author contributions: C.P. designed research; F.R., A. Bezvershenko, D.M., A. Bauer, M.G., A.R., and C.P. performed research; F.R., A. Bezvershenko, D.M., A. Bauer, M.G., A.R., and C.P. analyzed data; and F.R., A. Bezvershenko, D.M., A. Bauer, M.G., A.R., and C.P. wrote the paper.

The authors declare no competing interest.

This article is a PNAS Direct Submission.

[1]F.R. and A. Bezvershenko contributed equally to this work.

[2]To whom correspondence may be addressed. Email: christian.pfleiderer@tum.de.

This article contains supporting information online at https://www.pnas.org/lookup/suppl/doi:10.1073/pnas.2507428123/-/DCSupplemental.

Published January 29, 2026.

the skyrmion is described by virtue of an emergent magnetic field, that accounts for the deflection of conduction electrons and the concomitant appearance of a topological Hall effect of electrons traversing a skyrmion lattice (12, 25–27). The resulting counterforce on the skyrmion may exceed the pinning forces due to disorder such that the skyrmions start to move (11, 12). In cubic chiral magnets, the precise microscopic origins of the pinning potentials are unknown. In magnetic multilayers, the effective disorder potential was explored by measuring the thermally activated diffusion of individual skyrmion bubbles (28). However, the pinning of a skyrmion lattice is expected to differ qualitatively from that of individual skyrmion bubbles as the stiffness of the lattice renormalizes the pinning potentials (29).

Intimately connected to the spin-current-driven motion of skyrmions is the physics of their depinning (29, 30) and their dynamical response (31–33). For instance, an emergent electric field was observed with the onset of skyrmion motion (12, 34, 35), and the current-induced deformation dynamics of moving skyrmion strings was tracked by means of the second-harmonic Hall effect (36). Moreover, techniques such as small-angle neutron scattering (37, 38), ultrasound spectroscopy (20), and transmission electron or X-ray microscopy (39, 40) were combined with numerical methods to study the current-driven depinning, deformation, and creep of skyrmion lines (41–45). In this context, open questions are whether skyrmion lines remain intact or break up into pieces by virtue of Bloch points and how they interact with surfaces (46–52).

To explore the properties of a skyrmion lattice under simultaneous application of spin transfer torques and dynamic changes of orientation, we measured the transverse susceptibility of MnSi. This compound represents the perhaps most extensively studied and best understood metallic skyrmion-hosting material. The unpinning of the skyrmion lattice under either electric currents or oscillations of the magnetic field direction has been demonstrated previously in MnSi (11, 21) but electric currents and magnetic field oscillations had not been combined.

As our main new result we identify, track, and interpret two key signatures: first, an increase of the real part of the susceptibility χ as the skyrmion lattice becomes unpinned and responds better to the probing field, and second, the emergence of dissipation with the onset of unpinning, encoded in a rise of the imaginary part of χ, followed by a reduction of the dissipation once the skyrmions are depinned completely. We use measurements of a thermodynamic quantity, namely the magnetic AC susceptibility, in the presence of electrical currents as an unusual approach to track the depinning transition and thus the motion of skyrmions. Our experimental results are in remarkable qualitative and semiquantitative agreement with an effective slip-stick model of the bending and motion of the skyrmions. This permits the prediction of several dynamical skyrmion lattice phases representing phases of matter far from thermal equilibrium not created and observed before.

Results

In our study, we consider a static magnetic field in the z direction, B_z, that is combined with a slowly oscillating field with small amplitude, b, in the x direction, $\boldsymbol{B}(t) = (B_x(t), 0, B_z)$ with $B_x(t) = b\cos(\omega t)$. We consider frequencies ω in the range of a few hertz up to a few kilohertz, which is much smaller than the gigahertz regime of typical magnons (53, 54).

When slowly changing the direction of the field in the absence of pinning, the skyrmion lines follow the applied field (10), tilting

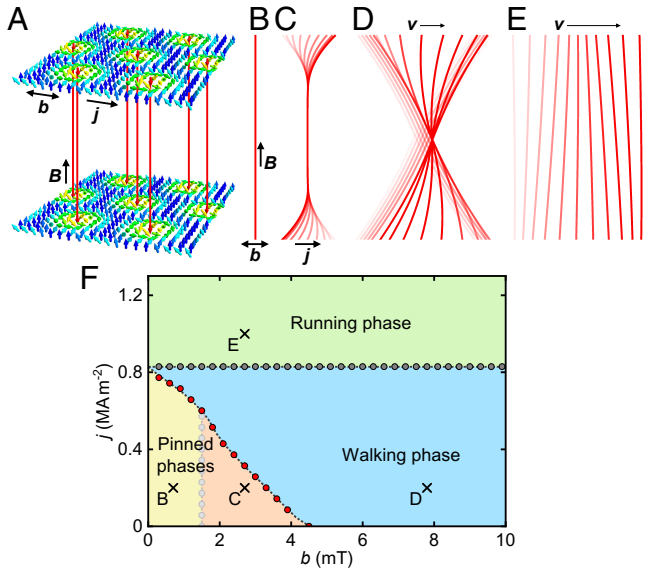

Fig. 1. Characteristics of skyrmion motion when an oscillating magnetic field b and an electrical current density j are applied perpendicular to the skyrmion lines. (*A*) Depiction of the skyrmion lines forming along the static magnetic field $\boldsymbol{B}$ in a trigonal lattice. (*B–E*) Stroboscopic visualization of the bending and motion of a skyrmion string in the plane spanned by $\boldsymbol{B}$ and $\boldsymbol{b}$ for different values of b and j. Decreasing color saturation encodes the progress of time. In the fully pinned phase (FPP, B), the skyrmion string is static. In the partially pinned phases (PPP, C), only the ends of the string move. In the walking (WP, D) and running phases (RP, E), a net translational velocity v is observed. In the WP, a part of the string is not moving during parts of the time evolution. In the RP, the entire string moves. (*F*) Phase diagram of skyrmion motion obtained from simulations of Eq. **1** using parameters $\epsilon_0/LF^{p,b} = 36.7$, $\omega/\omega_0 = 1.26$, $F^{p,st}/(LF^{p,b}) = 0.2$, $\alpha\mathcal{D}/\mathcal{G} = 0.1$, and $\beta\mathcal{D}/G = 0.07$ (see *SI Appendix* for details). Crosses denote the field b and current j values visualized in B–E.

by a small angle $\alpha \approx B_x(t)/B_z$. As a consequence, the ends of the skyrmion line will move a macroscopically large distance $\sim L\alpha/2$, where $\alpha \ll 1$ is the tilt angle of the magnetic field and L the length of the skyrmion line.

In the presence of pinning, in contrast, whether and how the skyrmion lines follow the field direction depends on the amplitude b and the frequency ω of the oscillating field. For small amplitudes, the orientation of the skyrmion line does not change. The associated magnetic texture deforms only slightly as described by standard linear-response theory. For large amplitudes, the skyrmion lines depin and follow the magnetic field, as previously reported (21).

As depicted in Fig. 1*A*, the interplay of slow oscillations of the direction of the magnetic field by a small transverse magnetic field, b, with an applied electric current density, j, leads to a rich nonequilibrium phase diagram already at the level of mean-field calculations (see *Discussion* for details). At least four different phases may be distinguished: i) In the fully pinned phase (FPP, Fig. 1*B*), all parts of the skyrmion lines are static at all times with the exception of the tiny oscillations associated with magnons (not depicted in the figure). ii) In the partially pinned phase (PPP, Fig. 1*C*), macroscopic parts of the skyrmion lines unpin and follow the applied field, while other parts remain pinned. iii) In the walking phase (WP, Fig. 1*D*), all parts of a skyrmion line move over the course of a field oscillation, but remain pinned during a finite fraction of the oscillation period. We name this phase in loose analogy to the motion of humans, where walking implies that at each time at least one foot is on the ground and thus not moving. iv) In the running phase

(RP, Fig. 1*E*), all parts of the skyrmion line are unpinned and move at all times of an oscillation.

A crucial difference of the unpinned phases as compared to the pinned phases concerns the response to an applied electric current. In the walking and the running phase arbitrarily small currents cause a net motion of the skyrmion lines despite the presence of disorder. On a related note, for micrometer-sized skyrmion bubbles in magnetic multilayers a 300-fold increase of the diffusion constant was reported under oscillations of the magnetic field (55). Most likely, however, this increase reflects a crossover rather than a pinning–depinning phase transition as observed in our study. Compared to the macroscopic motion of the ends of skyrmion strings induced by the oscillating field in MnSi, the domain wall motion in the multilayers remains restricted to much smaller distances (55).

Shown in Fig. 1*F* is the diagram of dynamical phases as a function of oscillation amplitude and current density. At vanishingly small oscillation amplitude, the FPP of the skyrmion lattice undergoes a complete unpinning into the RP above a critical current density j_c. At zero current density, an increasing oscillation amplitude induces a transition from the FPP to the PPP, followed by the transition from the PPP to the WP. Under increasing current density, the oscillation amplitude necessary to induce the transition into the WP is reduced. Independent of the oscillation amplitude, above j_c the WP is transformed into the RP.

Before turning to our experiments, we recall that the magnetic phase diagram of MnSi includes different static magnetic phases at a temperature suitable for our study (56). As a function of increasing magnetic field helical order, conical order, the skyrmion lattice, conical order, and the field-polarized (ferromagnetic) state are stabilized.

For information on the experimental set-up, the precise conditions of our measurements, the correction of heating effects, and the data reduction, we refer to *Materials and Methods* and *SI Appendix*. Shown in Fig. 2 *A* and *B* are the real and the imaginary parts of the transverse susceptibility, $\mathrm{Re}\chi^{\perp}$ and $\mathrm{Im}\chi^{\perp}$, as a function of the magnetic field B at 28.1 K for different current densities j. Starting from the helical state at $B = 0$, a pronounced peak at B_{c1} marks the transition to the conical state. At the lower and upper transition fields of the skyrmion lattice state at B_{a1} and B_{a2}, changes of slope are observed. Above a kink at B_{c2}, the field-polarized state is entered.

In the field range of the skyrmion lattice state, $B_{a1} < B < B_{a2}$, both $\mathrm{Re}\chi^{\perp}$ and $\mathrm{Im}\chi^{\perp}$ increase monotonically under increasing j. In comparison, in the helical and conical states, no dependence on j was observed. Relative changes of the real and the imaginary part of the susceptibility with respect to $j = 0$ under various current densities are depicted in gray shading in Fig. 2 *C* and *D*. Data at $j = 0$ are consistent with previous reports of the transverse susceptibility (57, 58).

We turn now to the two limiting ways of unpinning the skyrmion lattice (SkX), namely either by virtue of an electric current or oscillations of the applied field, as shown in Fig. 3 *A* and *B* or *C* and *D*, respectively. For ease of comparison, additional data recorded in the helical (Hel), conical (Con), and field-polarized (FP) states are shown.

In the skyrmion lattice phase at 0.22 T, both $\Delta_{j=0}\mathrm{Re}\chi^{\perp}$ and $\Delta_{j=0}\mathrm{Im}\chi^{\perp}$ display essentially the same three key characteristics as a function of increasing j as shown in Fig. 3 *A* and *B*. Namely, the susceptibility i) is unchanged up to a critical current density $j_c \approx 0.5\,\mathrm{MA\,m^{-2}}$, ii) displays an abrupt increase for $j > j_c$, followed iii) by a sublinear increase approaching a saturation for $j \gg j_c$. In the helical and conical states, recorded at 0.01 T and 0.30 T, respectively, the susceptibility remains essentially unchanged, where the small increase of $\Delta_{j=0}\mathrm{Re}\chi^{\perp}$ in the helical state (Fig. 3*A*) may be related to small systematic errors of the correction of the ohmic heating (cf. *SI Appendix*).

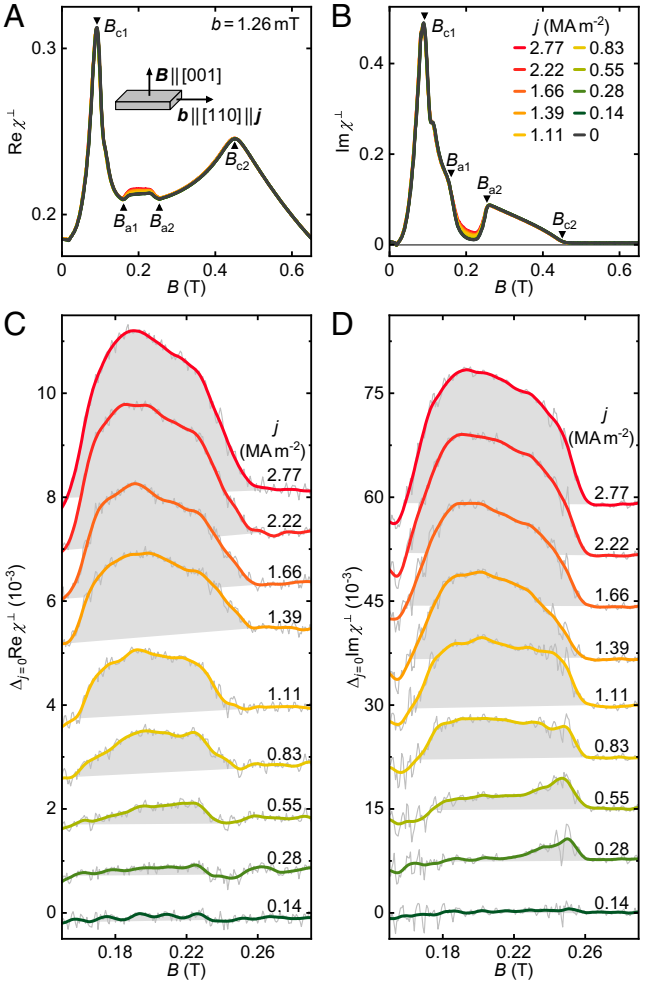

Fig. 2. Transverse susceptibility of MnSi as a function of static magnetic field, B, across the different magnetic states under various applied current densities j for a medium-sized oscillating field, $b = 1.26$ mT measured at the frequency $f = 120$ Hz. (*A*) Real part, $\mathrm{Re}\,\chi^{\perp}$, and (*B*) imaginary part, $\mathrm{Im}\,\chi^{\perp}$, of the transverse susceptibility. Changes of slope, labeled B_{c1}, B_{a1}, B_{a2}, and B_{c2}, indicate the transitions between the equilibrium magnetic states, see text for details. Applied currents increase the transverse susceptibility for $B_{a1} < B < B_{a2}$, i.e., in the skyrmion lattice state. (*C* and *D*) Change of the real and imaginary part relative to the values observed without current, $\Delta_{j=0}\mathrm{Re}\chi^{\perp}$ and $\Delta_{j=0}\mathrm{Im}\chi^{\perp}$, in the field range of the skyrmion lattice state. Data were offset for better visibility.

Qualitatively, $\Delta_{j=0}\mathrm{Re}\chi^{\perp}$ and $\Delta_{j=0}\mathrm{Im}\chi^{\perp}$ agree well with the behavior calculated theoretically presented below. Quantitatively the value of j_c corresponds quite well to current densities in small-angle neutron scattering and the Hall effect which established first that the skyrmion lattice starts to move freely (11, 12). As the skyrmions are unpinned from disorder, they adjust to the small excitation field and the susceptibility increases. Thus, these characteristics in the susceptibility represent the signature of the unpinning of the skyrmion lattice under an electric current. Indicated in color shading in Fig. 3 are the dynamical phases under increasing j, notably the FPP (yellow) and the RP (green). The transition must include a small regime of WP (blue) we cannot distinguish further.

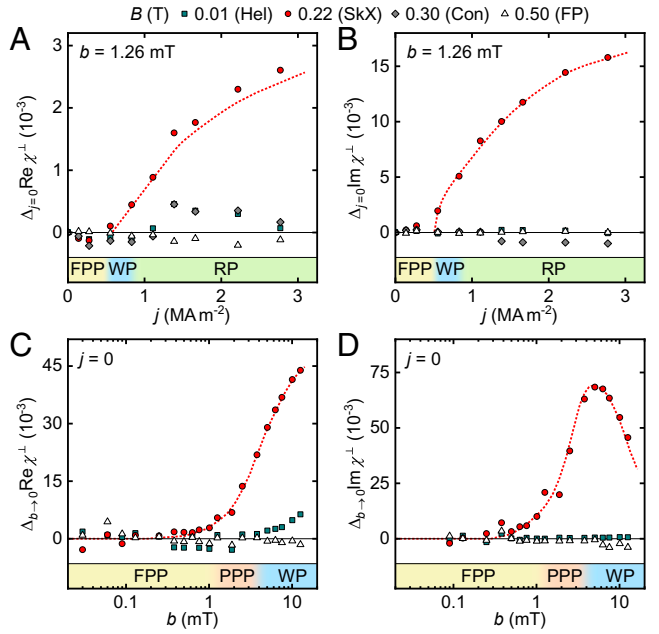

Fig. 3. Changes of the transverse susceptibility, $\chi^{\perp}$, in the different magnetic equilibrium states in MnSi under different applied current densities, j, and oscillating fields, b. Static field values, B, are representative of the helical (Hel, squares), skyrmion lattice (SkX, circles), conical (Con, diamonds), and field-polarized state (FP, triangles). Depicted in color shading below each panel are the different dynamic phases, namely the fully pinned phase (FPP), the partially pinned phase (PPP), the walking phase (WP), and the running phase (RP). (*A* and *B*) Change of the real and imaginary part as a function of current density relative to the values observed without current, $\Delta_{j=0}\mathrm{Re}\chi^{\perp}$ and $\Delta_{j=0}\mathrm{Im}\chi^{\perp}$. The oscillating field was $b = 1.26$ mT. (*C* and *D*) Change of the real and imaginary part as a function of the oscillation amplitude relative to the values observed at vanishing amplitude, $\Delta_{b\to 0}\mathrm{Re}\chi^{\perp}$ and $\Delta_{b\to 0}\mathrm{Im}\chi^{\perp}$. No current was applied, $j = 0$.

Shown in Fig. 3 *C* and *D* are $\Delta_{j=0}\mathrm{Re}\chi^{\perp}$ and $\Delta_{j=0}\mathrm{Im}\chi^{\perp}$ as a function of oscillation amplitude, b, at $j = 0$. The key characteristics observed as a function of b are similar though not identical to those observed under increasing j. Namely, $\Delta_{j=0}\mathrm{Re}\chi^{\perp}$ and $\Delta_{j=0}\mathrm{Im}\chi^{\perp}$ are unchanged up to a critical amplitude $b_c \approx 0.7$ mT. They initially exhibit a monotonic increase for $b > b_c$. However, $\Delta_{j=0}\mathrm{Re}\chi^{\perp}$ and $\Delta_{j=0}\mathrm{Im}\chi^{\perp}$ display a point of inflection and a maximum, respectively, around $b^* \approx 5$ mT beyond which they do not track each other. In comparison to the skyrmion lattice phase (SkX), data recorded in the helical phase (Hel) at 0.01 T and conical phase (Con) at 0.30 T are essentially constant as a function of b.

The dependence on oscillation amplitude is also in remarkable qualitative agreement with the theoretical calculation presented below. The unpinning permits the skyrmions to align better with the applied field, resulting in an increase of the real part of the susceptibility. The maximum observed in $\Delta_{j=0}\mathrm{Im}\chi^{\perp}$ reflects the decreases of dissipation as the skyrmions become fully unpinned. The color shading denotes the field range of the FPP (yellow), the PPP (orange), and the WP (blue). As $j = 0$, the skyrmions are walking on the spot in the WP. Underscoring this interpretation quantitatively, the value of $b_c \approx 0.7$ mT translates to a tilting angle of ~0.2° compared to a tilting angle for unpinning ~0.4° observed microscopically in TISANE (21).

The main result of our study is finally obtained when combining different current densities with different field oscillation amplitudes. Most notably, Fig. 4 establishes that sufficient shaking of the skyrmion lattice by the oscillating field, namely $b > b^*$, induces a phase with vanishing depinning current. Shown in Fig. 4*A* is $\Delta_{j=0}\mathrm{Re}\chi^{\perp}$ as a function of current density for different oscillation amplitudes b. The critical current density j_c at small amplitudes is defined as the point where $\Delta_{j=0}\mathrm{Re}\chi^{\perp}$ increases abruptly (red triangles). Under increasing b, j_c decreases and vanishes abruptly for $b > b^*$, indicating the transition into the walking phase with $j_c = 0$. In Fig. 4*B*, this evolution of j_c is compared with the change of the susceptibility induced by b at $j = 0$ as already presented in Fig. 3 *C* and *D*. Combining the change of both the real and the imaginary part for the skyrmion lattice highlights that as j_c vanishes for $b > b^*$, $\Delta_{b\to 0}\mathrm{Im}\chi^{\perp}$ shows a maximum while $\Delta_{b\to 0}\mathrm{Re}\chi^{\perp}$ exhibits a point of inflection.

Discussion

For a minimal theoretical description of our experimental observations, we developed a theory which includes i) nonlinear effects due to the coupling of a skyrmion line to a magnetic

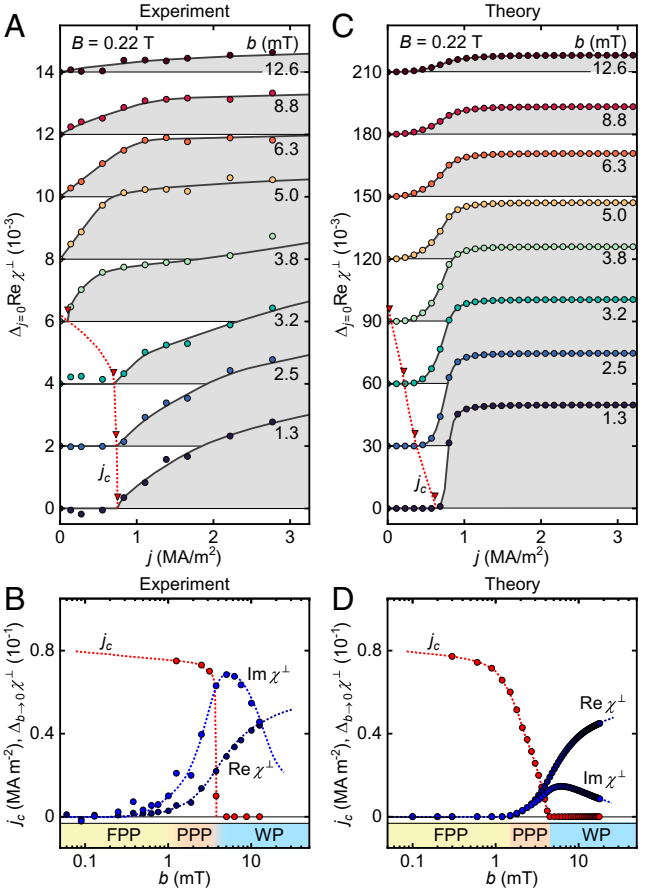

Fig. 4. Suppression of the critical current density, j_c, of skyrmion lattice flow under transverse oscillating field, b. (*A* and *B*) Experimental results are compared with (*C* and *D*) theoretical calculations. The skyrmion lattice state was stabilized at the static magnetic field $B = 0.22$ T. (*A* and *C*) Change of the real part of the transverse susceptibility as a function of current density j relative to the values observed without current, $\Delta_{j=0}\mathrm{Re}\chi^{\perp}$, for different oscillation amplitudes, b. (*B* and *D*) Change of the real and imaginary part of the transverse susceptibility (blue symbols) as function of the oscillation amplitude relative to the values observed at vanishing amplitude, $\Delta_{b\to 0}\mathrm{Re}\chi^{\perp}$ and $\Delta_{b\to 0}\mathrm{Im}\chi^{\perp}$, when no current is applied, $j = 0$. When current and field oscillations are combined, the critical current density j_c of net translational motion of the skyrmion lines (red symbols) is suppressed to zero under increasing amplitude b, i.e., the walking phase is observed already at arbitrarily small current density. For the calculations, parameters were used as specified in the caption of Fig. 1.

field of oscillating direction, ii) the forces on the skyrmion lattice due to spin-polarized electric currents, and iii) an effective account of pinning by disorder. The effects of magneto-crystalline anisotropies are neglected being very weak in MnSi (10, 59).

We consider a small time-dependent transverse magnetic field component, $b\cos(\omega t)$, that induces a tilt of the skyrmion lattice assuming that the skyrmion lattice is free to move. To describe the tilting and any associated bending as well as a motion of the skyrmion lattice, we introduce a function $\boldsymbol{u}(z,t) = (u_x(z,t), u_y(z,t), z)$ which describes the displacement of skyrmion lines of length L, where z with $\frac{-L}{2} \leq z \leq \frac{L}{2}$ is a coordinate parallel to the skyrmion lines.

Assuming that the magnetization can be described by $\boldsymbol{M}(\boldsymbol{r},t) \approx \boldsymbol{M}_0(\boldsymbol{r} - \boldsymbol{u}(z,t))$ where $\boldsymbol{M}_0$ is the skyrmion lattice in equilibrium, we derive the Thiele equation for $u(z,t)$:

$$\mathcal{G}\times(\dot{\boldsymbol{u}}(z,t)-\boldsymbol{v_s})+\mathcal{D}(\alpha\dot{\boldsymbol{u}}(z,t)-\beta\boldsymbol{v_s}) = -\frac{\delta\mathcal{F}_u}{\delta\boldsymbol{u}(z,t)}+\boldsymbol{F}^{\text{pin}}. \quad [1]$$

Here, $\mathcal{G}$ is the gyrocoupling vector, $\mathcal{D}$ is the dissipative tensor, $\boldsymbol{v_s}$ is a (spin) drift velocity proportional to the applied electric current, α and β parameterize the Gilbert damping, and $\boldsymbol{F}^{\text{pin}}$ is an effective pinning force due to disorder. The free energy describing the alignment of the skyrmion lines parallel to the applied magnetic field is given by

$$\mathcal{F}_u \approx \frac{\epsilon_0}{2}\int_{-L/2}^{L/2} dz\left(\partial_z\boldsymbol{u} - \frac{\boldsymbol{B}_x(t)}{B}\right)^2, \quad [2]$$

where $\boldsymbol{B}_x(t) = b\cos(\omega t)\hat{\boldsymbol{x}}$ and ϵ_0 is an elastic constant parameterizing the stiffness of the skyrmion lattice. For an effective description of the effects of disorder, which proves to be essential in our study, we use a slip–stick model, where the pinning forces at the surface and in the bulk differ, similar to models previously applied to skyrmions (12) and superconducting vortices (60). At the surface of the sample, enhanced pinning is expected due to higher amounts of disorder and impurities. We refer to *SI Appendix* for details and derivations.

Eq. **1** represents an effective mean-field description of the bending and the translational motion of a skyrmion lattice, where fluctuation effects are ignored and disorder is not taken into account microscopically but only on average. Thus, this model captures the depinning transition only on a mean-field level and is not able to describe the behavior in regimes in which the physics of thermal creep or thermal activation (28) is important. Yet, as a mean-field theory, it captures the relevant phases and phase transitions. The rapid onset of the depinning transition observed in MnSi (12) suggests that thermal creep in fact is negligible.

As expressed in Eq. **2**, the transverse magnetic field, b, couples to the ends of the skyrmion string only, $\int_{-L/2}^{L/2}\partial_z\boldsymbol{u}dz = \boldsymbol{u}(L/2) - \boldsymbol{u}(-L/2)$. Thus, the transverse magnetic field enters only on the level of a boundary condition of Eq. **1**. Shown in Fig. 1 is the phase diagram when the pinning at both surfaces is identical but differs from the bulk. As presented in the introduction, one may then distinguish four phases, namely fully pinned (FPP), partially pinned (PPP), walking (WP), and running (RP). When the pinning at the surfaces differs in addition, calculations indicate that the partially pinned phase splits up into several subphases (see *SI Appendix* for details).

The key question pursued in our study concerned the signatures of the different dynamical phases and associated phase transitions in $\text{Re}\chi^\perp$ and $\text{Im}\chi^\perp$ as a function of oscillation amplitude b and electrical current density j. Shown in Fig. 4 *C* and *D* are changes of the calculated transverse susceptibility, $\Delta_{b\to 0}\text{Re}\chi^\perp$ and $\Delta_{b\to 0}\text{Im}\chi^\perp$, for a set of parameters chosen such that the values of the critical current density j_c at $b = 0$ and the real part of the susceptibility, $\text{Re}\chi^\perp$ at zero current match experiment. In these calculations, the critical current density is inferred on a microscopic level, namely above j_c the skyrmions exhibit net movement.

As a function of current density, the real part of the calculated susceptibility, $\Delta_{b\to 0}\text{Re}\chi^\perp$, shown in Fig. 4*C*, displays essentially all of the key characteristics observed experimentally. Namely, we observe i) no change up to j_c, ii) a pronounced increase at j_c, and iii) sublinear behavior approaching saturation for $j \gg j_c$. The same agreement is also seen in the imaginary part $\text{Im}\chi^\perp$ (cf. *SI Appendix*).

This evolution may be understood as follows. A constant current in the PPP causes a static deformation even in the presence of an oscillating magnetic field. Therefore, the difference $\Delta_{j=0}\chi^\perp(b,j) = \chi^\perp(b,j) - \chi^\perp(b,j=0)$, in both the real and imaginary part vanishes exactly within the PPP. Only when entering the WP or RP, the response measured by the real or imaginary part of $\Delta_{j=0}\chi^\perp(b,j)$ is affected by the current. Thus, the current response of $\Delta_{j=0}\chi^\perp$, shown for $\text{Re}\chi^\perp$ in Fig. 4*C*, permits to identify the transition into the WP.

Shown in Fig. 4*D* is the calculated amplitude dependence of $\text{Re}\chi^\perp$ and $\text{Im}\chi^\perp$ for $j = 0$ and of j_c as inferred from the current dependence shown in Fig. 4*C*. Again excellent qualitative agreement with experiment is observed. For small amplitudes, $b < 0.7$ mT, the skyrmion lattice is in the FPP. Under increasing amplitude, both $\text{Re}\chi^\perp$ and $\text{Im}\chi^\perp$, start to increase at the transition from the FPP to the PPP.

Further, the transition between the PPP and the WP for $j = 0$ does not exhibit a specific signature in the susceptibility (there is no net velocity in either phase). Instead a point of inflection in $\text{Re}\chi^\perp$ that coincides with the maximum in $\text{Im}\chi^\perp$ is predicted. Such a maximum in $\text{Im}\chi^\perp$ is indeed observed experimentally as shown in Fig. 4*B*. The decrease of $\text{Im}\chi^\perp$ and hence the decrease of dissipation following the maximum represents empirical evidence of the complete unpinning of the skyrmion lattice.

While our mean-field theory is in remarkable agreement with experiment overall, we also observe several discrepancies. The increase of $\text{Re}\chi^\perp$ as a function of current density observed experimentally is much smaller than in our theory (Fig. 4 *A* and *C*). Furthermore, in the walking phase, i.e., when j_c is suppressed to 0 at large amplitudes, theory predicts an analytic response to the current, $\Delta_{j=0}\text{Re}\chi^\perp \propto j^2$ for small j, while experiment suggests $\Delta_{j=0}\text{Re}\chi^\perp \propto |j|^\alpha$ with $\alpha \approx 1$.

A quantitative discrepancy is also visible in $\text{Im}\chi^\perp$ as a function of oscillation amplitude. While qualitatively the same field dependence is observed in our theory, the absolute value of dissipation is approximately a factor two larger in the experiment. Finally, values of j_c observed experimentally at intermediate values of b are larger than those calculated theoretically (Fig. 4 *B* and *D*).

A large part of the observed discrepancies may arise from the mean-field nature of our theory. The theory does not capture that only a fraction of skyrmions may move in the presence of currents and that moving skyrmion lattices becomes less disordered (29, 30). This may explain the nonanalytic onset of $\Delta_{j=0}\text{Re}\chi^\perp$ and the reduced amplitude of this quantity seen experimentally. Furthermore, an asymmetry of surface pinning

potentials may explain an increased amplitude of $\mathrm{Im}\chi^{\perp}$ and a more abrupt drop of j_c as a function of b (*SI Appendix*). Another potentially important effect is that skyrmion lines may break up into pieces as investigated numerically in ref. 48. The bending of skyrmion lines by the oscillating field, Fig. 1, and the associated elastic forces may favor such a breaking-up (*SI Appendix*, section 2H). As smaller skyrmion pieces can follow the magnetic field more easily, this leads to larger values of $\chi^{\perp}$ as a function of b as compared to the increase as a function of j.

Conclusions

When manipulating magnetic textures for the creation of novel nonequilibrium states of matter (61, 62), pinning by disorder is arguably one of the most important constraints. Access and control of pinning processes are of central importance for all skyrmion-based nonequilibrium properties as well as the creation of technologically useful skyrmion devices. In our study, we showed that periodically changing the magnetic field direction by just a few degrees provides access to dynamic phases in which pinning is effectively overcome. When combined with (spin) currents, a phase, in which skyrmions move at arbitrarily small current densities, becomes part of a rich phase diagram. The nonequilibrium character of these phases permits to resolve a wide range of fundamental and applied questions in future studies.

Materials and Methods

Sample Preparation. A single crystal of MnSi was grown by optical float-zoning under ultrahigh vacuum compatible conditions (63). X-ray Laue diffraction was used to orient the single crystal and a cuboid sample with dimensions 0.41 mm × 0.88 mm × 3.15 mm was cut using a wire saw. The largest face of the sample was normal to crystallographic ⟨001⟩ axis and the longest edge was parallel to a ⟨110⟩ axis. Current contacts were soldered to the smallest faces of the sample such that large current densities j could be applied parallel to [110].

Transverse Susceptibility. The transverse susceptibility under simultaneous application of electric currents was measured with a bespoke susceptometer in a superconducting magnet system equipped with a variable temperature insert. The primary of the susceptometer generated an oscillatory magnetic field $\boldsymbol{b}$ perpendicular to $\boldsymbol{B}$. A concentrically aligned balanced pair of secondaries recorded the transverse susceptibility, $\chi^{\perp}$, with respect to $\boldsymbol{B}$ (64). The sample, equipped with electrical contacts, was mounted on a sapphire platelet inside one of the secondaries such that $\boldsymbol{b}(t)$ and $\boldsymbol{j}$ were parallel. The combination of $\boldsymbol{B}$ and $\boldsymbol{b}$ resulted in oscillations of the field direction. Data were collected for an excitation frequency of $f = 120$ Hz and excitation amplitudes from less than 0.1 mT up to 12.6 mT. The maximum amplitude was limited by the effects of ohmic heating in the current leads and the primary. In the field range of the skyrmion lattice in MnSi, between 0.16 T and 0.26 T, the excitation amplitudes corresponded to small tilting angles of the total field below 5° while the field magnitude changed by less than 10^{-3} being essentially constant.

Further details of the experimental procedure, such as the calibration of the susceptometer, the thermal anchoring of the sample, the correction of heating effects, and considerations on the field homogeneity including contributions by the Oersted field due to the currents in the sample, are reported in *SI Appendix* and ref. 64.

Calculations. We use a simple phenomenological slip–stick model, similar to ref. 12, to describe pinning in Eq. **1**. A skyrmion stays pinned, $\dot{\boldsymbol{u}}(z,t) = 0$, when the external force at position z is smaller than a critical pinning force, $|\boldsymbol{F}(z)| \leq F^p$. In contrast, a moving skyrmion obtains a force $\boldsymbol{F}^p = -F^p(\dot{\boldsymbol{u}}/|\dot{\boldsymbol{u}}|)$ oriented antiparallel to its velocity. We allow for both bulk and surface pinning, $\boldsymbol{F}^{pin} = \boldsymbol{F}^{p,b} + \delta(z - L/2)\ \boldsymbol{F}^{p,s} + \delta(z + L/2)\ \boldsymbol{F}^{p,s}$. All numerical results are obtained by discretizing the model of Eq. **1** both in time and space ($\Delta z = L/60$, $\Delta t = 10^{-5}/f$, where $f = \omega/(2\pi)$ is the excitation frequency), see *SI Appendix* for further details.

There are effectively three fitting parameters for our theory, the dimensionless strength of bulk pinning $F^{p,b}L/(\epsilon_0)$, the ratio of surface to bulk pinning $F^{p,s}/(F^{p,s}L)$, and the characteristic frequency of the system $\omega_0 = \epsilon_0/(L^2\mathcal{G})$. Furthermore, we use $\alpha\mathcal{D}/\mathcal{G} = 0.1$ and $\beta/\alpha = 0.7$. The parameter $\epsilon_0 = 4 \cdot 10^{-13}$ J/m is obtained from susceptibility measurements, see *SI Appendix*, and $v_s \approx 10^{-4} j/j_c$ m/s, where $j_c \approx 10^6$ Am^{-2} has been estimated in ref. 12. This fixes all parameters of our model, including the absolute values of the susceptibilities and the values of the critical currents.

Data, Materials, and Software Availability. All study data are included in the article and/or *SI Appendix*.

ACKNOWLEDGMENTS. We wish to thank S. Mayr for fruitful discussions and assistance with the experiments. This study has been funded by the Deutsche Forschungsgemeinschaft (German Research Foundation) under CRC 1238 (Control and Dynamics of Quantum Materials, Project No. 277146847, subproject C04), CRC/TR 183 (Entangled States of Matter, Project No. 277101999, subproject A01), TRR80 (From Electronic Correlations to Functionality, Project No. 107745057), TRR360 (Constrained Quantum Matter, Project No. 492547816), SPP2137 (Skyrmionics, Project No. 403191981, Grant PF393/19), and the excellence cluster MCQST under Germany's Excellence Strategy EXC-2111 (Project No. 390814868). Financial support by the European Research Council through Advanced Grants No. 291079 (TOPFIT) and No. 788031 (ExQuiSid) is gratefully acknowledged.

Author affiliations: [a]Physik-Department, Technical University of Munich, Garching D-85748, Germany; [b]Institute for Theoretical Physics, Universität zu Köln, Köln D-50937, Germany; [c]Zentrum für QuantumEngineering, Technical University of Munich, Garching D-85748, Germany; [d]Institut für Theoretische Festkörperphysik, Karlsruhe Institute of Technology, Karlsruhe D-76131, Germany; [e]Institute for Quantum Materials and Technology, Karlsruhe Institute of Technology, Karlsruhe D-76131, Germany; [f]Heinz Maier-Leibnitz Zentrum, Technical University of Munich, Garching D-85748, Germany; and [g]Munich Center for Quantum Science and Technology, Technical University of Munich, Garching D-85748, Germany

1. A. Hubert, R. Schäfer, *Magnetic Domains: The Analysis of Magnetic Microstructures* (Springer, 1998).
2. B. Keimer, J. E. Moore, The physics of quantum materials. *Nat. Phys.* **13**, 1045 (2017).
3. F. Giustino *et al.*, The 2021 quantum materials roadmap. *J. Phys. Mater.* **3**, 042006 (2021).
4. R. Cava, N. de Leon, W. Xie, Introduction: Quantum materials. *Chem. Rev.* **121**, 2777 (2021).
5. N. Nagaosa, Y. Tokura, Topological properties and dynamics of magnetic skyrmions. *Nat. Nanotechnol.* **8**, 899 (2013).
6. B. Göbel, I. Mertig, O. A. Tretiakov, Beyond skyrmions: Review and perspectives of alternative magnetic quasiparticles. *Phys. Rep.* **895**, 1 (2021).
7. S. Mühlbauer *et al.*, Skyrmion lattice in a chiral magnet. *Science* **323**, 915 (2009).
8. X. Z. Yu *et al.*, Real-space observation of a two-dimensional skyrmion crystal. *Nature* **465**, 901 (2010).
9. L. J. Bannenberg *et al.*, Reorientations, relaxations, metastabilities, and multidomains of skyrmion lattices. *Phys. Rev. B* **96**, 184416 (2017).
10. T. Adams, M. Garst, A. Bauer, R. Georgii, C. Pfleiderer, Response of the skyrmion lattice in MnSi to cubic magnetocrystalline anisotropies. *Phys. Rev. Lett.* **121**, 187205 (2018).
11. F. Jonietz *et al.*, Spin transfer torques in MnSi at ultralow current densities. *Science* **330**, 1648 (2010).
12. T. Schulz *et al.*, Emergent electrodynamics of skyrmions in a chiral magnet. *Nat. Phys.* **8**, 301 (2012).
13. X. Z. Yu *et al.*, Skyrmion flow near room temperature in an ultralow current density. *Nat. Commun.* **3**, 988 (2012).
14. J. Zang, M. Mostovoy, J. H. Han, N. Nagaosa, Dynamics of skyrmion crystals in metallic thin films. *Phys. Rev. Lett.* **107**, 136804 (2011).
15. K. Everschor, M. Garst, R. A. Duine, A. Rosch, Current-induced rotational torques in the skyrmion lattice phase of chiral magnets. *Phys. Rev. B* **84**, 064401 (2011).
16. J. Iwasaki, M. Mochizuki, N. Nagaosa, Universal current-velocity relation of skyrmion motion in chiral magnets. *Nat. Commun.* **4**, 1463 (2013).
17. J. Seidel, Ed., *Topological Structures in Ferroic Materials: Domain Walls, Vortices and Skyrmions* (Springer, 2016).
18. S. Seki, M. Mochizuki, *Skyrmions in Magnetic Materials* (Springer, 2016).
19. S. Z. Lin, C. Reichhardt, C. D. Batista, A. Saxena, Particle model for skyrmions in metallic chiral magnets: Dynamics, pinning, and creep. *Phys. Rev. B* **87**, 214419 (2013).
20. Y. Luo *et al.*, Skyrmion lattice creep at ultra-low current densities. *Commun. Mater.* **1**, 1 (2020).
21. S. Mühlbauer *et al.*, Kinetic small angle neutron scattering of the skyrmion lattice in MnSi. *New J. Phys.* **18**, 075017 (2016).

22. D. Mettus, A. Chacon, A. Bauer, S. Mühlbauer, C. Pfleiderer, Optimization strategies and artifacts of time-involved small-angle neutron scattering experiments. *J. Appl. Crystallogr.* **55**, 1603 (2022).
23. P. Bruno, V. K. Dugaev, M. Taillefumier, Topological Hall effect and Berry phase in magnetic nanostructures. *Phys. Rev. Lett.* **93**, 096806 (2004).
24. W. Jiang *et al*., Direct observation of the skyrmion Hall effect. *Nat. Phys.* **13**, 162 (2017).
25. A. Neubauer *et al*., Topological Hall effect in the A phase of MnSi. *Phys. Rev. Lett.* **102**, 186602 (2009).
26. N. Nagaosa, Y. Tokura, Emergent electromagnetism in solids. *Phys. Scr.* **2012**, 014020 (2012).
27. C. Franz *et al*., Real-space and reciprocal-space Berry phases in the Hall effect of $Mn_{1-x}Fe_xSi$. *Phys. Rev. Lett.* **112**, 186601 (2014).
28. R. Gruber *et al*., Skyrmion pinning energetics in thin film systems. *Nat. Commun.* **13**, 3144 (2022).
29. C. Reichhardt, C. J. O. Reichhardt, M. V. Milošević, Statics and dynamics of skyrmions interacting with disorder and nanostructures. *Rev. Mod. Phys.* **94**, 035005 (2022).
30. C. Reichhardt, C. J. Olson Reichhardt, Depinning and nonequilibrium dynamic phases of particle assemblies driven over random and ordered substrates: A review. *Rep. Prog. Phys.* **80**, 026501 (2016).
31. S. Z. Lin, J. X. Zhu, A. Saxena, Kelvin modes of a skyrmion line in chiral magnets and the associated magnon transport. *Phys. Rev. B* **99**, 140408 (2019).
32. S. Seki *et al*., Propagation dynamics of spin excitations along skyrmion strings. *Nat. Commun.* **11**, 1 (2020).
33. V. P. Kravchuk, Nonlinear dynamics of skyrmion strings. *Phys. Rev. B* **108**, 144412 (2023).
34. D. Liang, J. P. DeGrave, M. J. Stolt, Y. Tokura, S. Jin, Current-driven dynamics of skyrmions stabilized in MnSi nanowires revealed by topological Hall effect. *Nat. Commun.* **6**, 8217 (2015).
35. M. T. Birch *et al*., Dynamic transition and Galilean relativity of current-driven skyrmions. *Nature* **633**, 554 (2024).
36. T. Yokouchi *et al*., Current-induced dynamics of skyrmion strings. *Sci. Adv.* **4**, eaat1115 (2018).
37. D. Okuyama *et al*., Deformation of the moving magnetic skyrmion lattice in MnSi under electric current flow. *Commun. Phys.* **2**, 1 (2019).
38. K. Ran *et al*., Bending skyrmion strings under two-dimensional thermal gradients. *Nat. Commun.* **15**, 4860 (2024).
39. F. S. Yasin *et al*., Real-space determination of the isolated magnetic skyrmion deformation under electric current flow. *Proc. Natl. Acad. Sci. U.S.A.* **119**, e2200958119 (2022).
40. M. T. Birch *et al*., Toggle-like current-induced Bloch point dynamics of 3D skyrmion strings in a room temperature nanowire. *Nat. Commun.* **13**, 3630 (2022).
41. S. Z. Lin, A. Saxena, Dynamics of Dirac strings and monopolelike excitations in chiral magnets under a current drive. *Phys. Rev. B* **93**, 060401 (2016).
42. F. Kagawa *et al*., Current-induced viscoelastic topological unwinding of metastable skyrmion strings. *Nat. Commun.* **8**, 1332 (2017).
43. W. Koshibae, N. Nagaosa, Bulk and surface topological indices for a skyrmion string: Current-driven dynamics of skyrmion string in stepped samples. *Sci. Rep.* **10**, 20303 (2020).
44. Z. Jin *et al*., Characteristics and applications of current-driven magnetic skyrmion strings. *Chin. Phys. Lett.* **39**, 108502 (2022).
45. S. Okumura, V. P. Kravchuk, M. Garst, Instability of magnetic skyrmion strings induced by longitudinal spin currents. *Phys. Rev. Lett.* **131**, 066702 (2023).
46. P. Milde *et al*., Unwinding of a skyrmion lattice by magnetic monopoles. *Science* **340**, 1076 (2013).
47. C. Schütte, A. Rosch, Dynamics and energetics of emergent magnetic monopoles in chiral magnets. *Phys. Rev. B* **90**, 174432 (2014).
48. W. Koshibae, N. Nagaosa, Dynamics of skyrmion in disordered chiral magnet of thin film form. *Sci. Rep.* **9**, 5111 (2019).
49. M. T. Birch *et al*., Topological defect-mediated skyrmion annihilation in three dimensions. *Commun. Phys.* **4**, 1 (2021).
50. R. Brearton, D. M. Burn, A. A. Haghighirad, G. van der Laan, T. Hesjedal, Three-dimensional structure of magnetic skyrmions. *Phys. Rev. B* **106**, 214404 (2022).
51. M. E. Henderson *et al*., Three-dimensional neutron far-field tomography of a bulk skyrmion lattice. *Nat. Phys.* **19**, 1617 (2023).
52. H. Jin *et al*., Evolution of emergent monopoles into magnetic skyrmion strings. *Nano Lett.* **23**, 5164 (2023).
53. Y. Onose, Y. Okamura, S. Seki, S. Ishiwata, Y. Tokura, Observation of magnetic excitations of skyrmion crystal in a helimagnetic insulator Cu_2OSeO_3. *Phys. Rev. Lett.* **109**, 037603 (2012).
54. T. Schwarze *et al*., Universal helimagnon and skyrmion excitations in metallic, semiconducting and insulating chiral magnets. *Nat. Mater.* **14**, 478 (2015).
55. R. Gruber *et al*., 300-times-increased diffusive skyrmion dynamics and effective pinning reduction by periodic field excitation. *Adv. Mater.* **35**, 2208922 (2023).
56. A. Bauer, C. Pfleiderer, Magnetic phase diagram of MnSi inferred from magnetization and ac susceptibility. *Phys. Rev. B* **85**, 214418 (2012).
57. A. Chacon *et al*., Uniaxial pressure dependence of magnetic order in MnSi. *Phys. Rev. Lett.* **115**, 267202 (2015).
58. Y. Nii *et al*., Uniaxial stress control of skyrmion phase. *Nat. Commun.* **6**, 8539 (2015).
59. A. Bauer *et al*., Symmetry breaking, slow relaxation dynamics, and topological defects at the field-induced helix reorientation in MnSi. *Phys. Rev. B* **95**, 024429 (2017).
60. D. B. Liarte *et al*., Vortex dynamics and losses due to pinning: Dissipation from trapped magnetic flux in resonant superconducting radio-frequency cavities. *Phys. Rev. Appl.* **10**, 054057 (2018).
61. R. Daviet, C. P. Zelle, A. Rosch, S. Diehl, Nonequilibrium criticality at the onset of time-crystalline order. *Phys. Rev. Lett.* **132**, 167102 (2024).
62. D. Hardt, R. Doostani, S. Diehl, N. del Ser, A. Rosch, Propelling ferrimagnetic domain walls by dynamical frustration. *Nat. Commun.* **16**, 3817 (2025).
63. A. Bauer, G. Benka, A. Regnat, C. Franz, C. Pfleiderer, Ultra-high vacuum compatible preparation chain for intermetallic compounds. *Rev. Sci. Instrum.* **87**, 113902 (2016).
64. F. Rucker, "Transverse susceptibility of complex magnetic textures," PhD thesis, Technische Universität München (2017), http://mediatum.ub.tum.de/?id=1452722.